
# Deposition of titanium films on complex bowl-shaped workpieces using DCMS and HiPIMS

Dong Xie, L.J. Wei, H.Y. Liu, K. Zhang, Y.X. Leng, D.T.A. Matthews, R. Ganesan, Y.Y. Su

PII: S0257-8972(22)00113-X

DOI: https://doi.org/10.1016/j.surfcoat.2022.128192

Reference: SCT 128192

To appear in: *Surface & Coatings Technology*

Received date: 6 January 2022

Revised date: 27 January 2022

Accepted date: 28 January 2022

Please cite this article as: D. Xie, L.J. Wei, H.Y. Liu, et al., Deposition of titanium films on complex bowl-shaped workpieces using DCMS and HiPIMS, *Surface & Coatings Technology* (2021), https://doi.org/10.1016/j.surfcoat.2022.128192

# Deposition of titanium films on complex bowl-shaped workpieces using DCMS and HiPIMS[1]

Dong. Xie[a], L.J. Wei[a], H.Y.Liu[b], K. Zhang[b], Y.X. Leng[b,*], D.T.A. Matthews[c,d*], R. Ganesan[e,*], Y.Y. Su[f]

[a] Key Laboratory of Advanced Technologies of Materials, Ministry of Education of China, School of Physical Science and Technology, Southwest Jiaotong University, Chengdu 610031, China

[b] Sichuan Province International Science and Technology Cooperation Base of Functional Materials, School of Materials Science and Engineering, Southwest Jiaotong University, Chengdu 610031, China

[c] Department of Mechanics of Solids Surfaces and Systems, Faculty of Engineering Technology, The University of Twente, The Netherlands

[d] Department of Materials Science & Engineering, Feng Chia University, Taiwan,China

[e] School of Physics, University of Sydney, Sydney, NSW 2006, Australia

[f] Research Institute for New Materials Technology, Chongqing University of Arts and Sciences, Chongqing 402160, China

Email: yxleng@home.swjtu.edu.cn

Email: d.t.a.matthews@utwente.nl

Email: rajesh.ganesan@sydney.edu.au

**Abstract**: Herein, the deposition of titanium films on complex bowl-shaped workpieces was conducted using direct-current magnetron sputtering (DCMS) and high-power impulse magnetron sputtering (HiPIMS) methods, and the differences in the properties of the film deposited using these methods were investigated. Metallic titanium films were deposited on the inner (concave) and outer (convex) surfaces of a bowl-shaped workpiece. The deposition

[1] Abbreviations. HiPIMS: high-power impulse magnetron sputtering; DCMS: direct-current magnetron sputtering; PVD: physical vapor deposition; XRD: X-ray diffraction; SEM: scanning electric microscopy; EDS: energy dispersive X-ray spectroscopy

rate, crystal structure, microhardness, and cross-sectional morphology of the titanium films at different deposition angles with respect to the normal vector of the target surface were characterized. Results showed that HiPIMS films exhibited better uniformity in terms of the crystal texture, microhardness, and microstructure than that of DCMS films, for both concave and convex surfaces. The differences between the properties of the HiPIMS and DCMS deposited films can be attributed to the significantly reduced self-shadowing effect in the oblique incidence deposition provided by HiPIMS. The enhanced energetic bombardment of depositing species on the substrate in the ionization-rich HiPIMS plasma facilitates the deposition films with uniform crystal structures and properties. However, a distinct difference in the film deposition rates was observed for the different shapes of the substrates in both deposition techniques. The films deposited on concave surfaces showed better uniformity than that of the films deposited on convex surfaces. This phenomenon can be explained by considering both the effect of the substrate-to-target distance, line of sight and the electric field near the substrate. The results presented in this manuscript are therefore crucial for the coating design of objects with complex shapes when depositing pure metals using DCMS and/or HiPIMS for decorative, tribological, and tool applications.

**Keywords:** film uniformity, bowl-shaped workpiece; direct-current magnetron sputtering; high-power impulse magnetron sputtering; oblique incidence deposition

## 1. Introduction

Magnetron sputtering is a widely utilized PVD method that aims to improve properties such as wear and corrosion resistance in a wide range of products and applications [1]. However, for conventional DCMS, the effects of oblique deposition and self-shadowing repeatedly exist when the film is deposited on complex-shaped workpieces [2-3]. Various strategies have been reported to negate these effects, such as rotating or swinging the workpiece; however, the oblique deposition effect cannot be completely eliminated. Furthermore, it is often difficult to sufficiently manipulate large workpieces due to the limited space of the vacuum chamber. It is

commonly known that oblique deposition will affect the growth of films, thereby negatively influencing the uniformity of the film structure and the properties of the films deposited on complex-shaped workpieces [4-5]; this ultimately leads to unpredictable and reduced product performance. Therefore, it is critical to thoroughly analyze the uniformity of the films deposited on the whole complex-shaped workpiece to evaluate and predict the service life of the workpiece and/or propose an optimal solution for the weakest area of the film.

HiPIMS is an ionized PVD technique [6], during which sputtered atoms have a high degree of ionization, and their energy and trajectory can be modulated using an external electric or magnetic field [7-8]. This makes it possible to deposit dense and smooth coatings on complex-shaped substrates. Some metal and ceramic films have been deposited on complex components, such as trenches [9-10], cutting tools [11], or gear wheels [12], using both DCMS and HiPIMS methods. Better uniformity in terms of the film thickness was observed in HiPIMS[13]. However, most studies are limited to the concave surface of a workpiece, and those focusing on both the convex and concave surfaces of complex workpieces are scarce.

A major sector that delivers products with such complex shapes is the decorative market, which was estimated to have a value of US$ 86 billion at the end of 2019 that further increased to US$ 112 billion in 2021. It is expected to significantly rise by 4.61% per year between 2021 and 2028 [14]**.** PVD technology holds a significant share in the decorative coating market.

Although decorative coatings deposited using PVD processes are typically focused on arc-based processes, new coating processes focus on the HiPIMS and DCMS of titanium-based targets for more challenging colors. Typical decorative parts coated using HiPIMS processes include door handles, faucet parts, and other consumer items with 3D shapes, or freeform surfaces. It is therefore critical to study the thickness, structure, and nature of growing films on complex-shaped workpieces.

Considering the above points, herein, a bowl-shaped workpiece is utilized as a model workpiece to study the angular dependence of the structure and the properties of the films generated during magnetron sputtering. Titanium has advantages of excellent corrosion resistance and biocompatibility [15-16] and is a major source of cathode material for many colors in decorative PVD coating applications. In addition, titanium films are widely used as buffer layers in many practical applications to improve the adhesive force between ceramic films and metal substrates [17-18]. For these reasons, titanium films were selected for deposition on Si-wafers positioned within a stainless-steel bowl-shaped workpiece. The deposition angles with respect to the surface normal of the target continuously changed from 0° to 90°. The films were characterized using their thickness, crystal structure, microhardness, cross-sectional morphology, and deposition rate at different deposition angles on the bowl-shaped workpiece. The uniformity of the characteristics of the titanium film over the entire workpiece during both DCMS and HiPIMS was evaluated and compared, and the differences are discussed.

## 2. Material and methods

The deposition of the titanium film was performed in a vacuum deposition system, which is described elsewhere [20]. The high-vacuum deposition system was equipped with four rectangular unbalanced magnetrons, and the size of the rectangular target (Ti 99.9 %) was 135 mm × 170 mm. The schematic of the deposition system is illustrated in fig.1. During deposition, the target cathode labeled B ( as shown in fig.1) was powered by a DC or pulsed power supply, manufactured by the Chengdu Pulsetech Electrical Company (HPS-450D, China). Although the other three targets was not used in present study, the magnetic field configuration behind them also plays a role during magnetron sputtering[21-22].

A stainless-steel bowl-shaped workpiece 10 cm in diameter and 1 mm in thickness is selected as the specimen holder. To investigate the titanium film deposited on the different areas of the

complex-shaped workpiece, seven Si(100) wafers (n-type) were mounted on the surfaces of the bowl-shaped substrate from the brim to the bottom, as shown in Fig.2. The size of the Si wafer was 20 mm × 10 mm, and the silicon wafers were labeled L-90°, L-60° L-30° M-0°, R-30°, R-60°, and R-90°, corresponding to the deposition angles of 90°, 60°, 30°, and 0°, respectively, where L-, R-, and M- denote left, right, and middle, respectively. Film characterization was conducted on these Si wafers, and the test results were used to evaluate the uniformity of films. The distance from the target to the top of bowl-shaped substrate was set to 60 mm, and the center of the bowl-shaped workpiece was aligned to the target center, as shown in Fig.2.

Prior to film deposition, the base pressure of the vacuum chamber was set to $1.0 \times 10^{-3}$ Pa. Thereafter, the argon pressure was adjusted to 0.6 Pa in the chamber. For the DCMS process, the target voltage was set to −300 V with a current of 3 A. For the HiPIMS process, a constant voltage pulse of −800 V was applied with a pulse length (τ) of 400 μs and a corresponding frequency (f) of 100 Hz. The operating parameters in HiPIMS were selected to ensure that the average power applied to the target in DCMS was achieved. The deposition times for HiPIMS and DCMS were restricted to 30 and 10 min, respectively. Different deposition times were used to maintain almost the same film thickness at the center position normal to the target in the DCMS and HiPIMS processes. The bias voltage applied to the workpiece was set to −50 V in both the DCMS and HiPIMS processes.

A surface profiler (AMBIOS model XP-2, USA) was used to measure the thicknesses of deposited films. The crystal texture of the titanium films was characterized using XRD (PHILIPS PW 3040) with Cu Kα radiation (40 kV, 40 mA). The scanned 2θ range was 30°–48° in the conventional Bragg–Brentano geometry mode. The cross-sectional morphologies of titanium films were observed using SEM (Jeol JSM-7001F, Japan), and the composition of deposited films were measured using EDS (FEI Quanta 250 FEG, USA). Microhardness was measured using an ultra-micro hardness tester (Shimadzu DUH211S, Japan), with a

Vickers-shaped diamond indenter operated at a loading/unloading rate of 0.7316 mN/s, while the holding time at the maximum load (10 mN) was set to 10 s.

## 3. Results and discussion

### 3.1. Film deposition rate

The deposition rates of the titanium films at different deposition angles on the inner and outer surfaces of the bowl-shaped workpiece are shown in Figs.3a and 3b, respectively. The deposition rate of HiPIMS is consistently lower than that of DCMS, whether the film is deposited on the inner (concave) or outer (convex) surface. These results are in agreement with the findings of other studies [9]. A prevalent explanation for the lower deposition rate in HiPIMS is that most sputtered ionized particles, which are positively charged, will be attracted back to the target owing to a larger negative potential on the target [23-24]. When a film is deposited on the concave surface, the deposition rate of the films deposited using DCMS increases with increasing deposition angles. However, for the HiPIMS films on the concave surface, an opposite trend is observed, as shown in Fig.3a. For the films deposited on the convex surface of the workpiece, the deposition rates in HiPIMS and DCMS exhibit the same distribution trend. The distribution of films using both methods decreases with increasing deposition angles, as observed in Fig.3b. This is similar to HiPIMS on the concave surface, but the change on the convex surface is more pronounced than that on the concave surface.

The deposition rate is sensitive to the distance from the target to the substrate during magnetron sputtering [25-26]. It was known that when sputtered atoms (particles) fly to the substrate, they experience collisions with ambient gases and are decelerated until they are equilibrated with the gases. With the increase of the target to substrate distance, the number of collisions between the sputtering particles and the gas molecules increases, , and the transport manner of the sputtered atoms (particles) will change from “ballistic” to “diffusive” [27]. In the diffusive transport model, sputtered particles travel randomly and their the flux at the

substrate decreases monotonically with the target and substrate distance[27]. For these reasons, the deposition rate decreases with an increasing substrate-to-target distance. As shown in Fig.2a, on the concave surface, the distance between Si wafers and the target decreases with increasing deposition angles. However, on the convex surface, the distance increases with increasing deposition angles. Therefore, the distribution of the film deposition rates on the inner and outer surfaces can be explained using this effect of the substrate-to-target distance. However, the distribution of the deposition rate for the HiPIMS film on the concave surface shows a contradictory result as it exhibits a slight increase with an increasing target-to-substrate distance. In the HiPIMS process, most sputtered atoms are ionized particles, so their energy and trajectory will be affected by the external electric field near the substrate. Hippler et al. [28] tested the distribution of the plasma potential in a semicircular copper holder during HiPIMS discharge. It was found that the drop in the plasma potential at lower deposition angles was larger than that at higher deposition angles, suggesting that more ionized particles were attracted to the positions associated with lower deposition angles (such as M-0° in Fig.2). Additionally, the slightly higher deposition rate at lower deposition angles can be explained by considering both the effect of the substrate-to-target distance, line of sight and the electric field near the substrate.

The equation, $N = \frac{d_{min}}{d_{max}} \times 100\%$, [29] was used to quantitatively evaluate the uniformity of the film on the entire inner or outer surface of the workpiece. With $d_{min}$ and $d_{max}$ representing the minimum and maximum deposition rates on the same surface, respectively, the uniformity of the film deposition rate on the concave surface of the workpiece was calculated to be 82.7% and 89.8% for DCMS and HiPIMS, respectively. However, on the convex surface, this rapidly dropped to 14.3% and 17.6% for DCMS and HiPIMS, respectively, as shown in Fig.4. The calculated results suggest that the uniformity of the film deposition rate on the workpiece was significantly affected by the shape of the surface. The

uniformity of the film deposition rate on the concave surface is much better than that of the film deposition rate on the convex surface. However, on the same surface, the HiPIMS film always exhibits a slightly better uniformity in terms of the film deposition rate. It is known that the sputtered atoms in the HiPIMS method have a higher degree of ionization and a more enhanced particle bombardment effect than those of the sputtered atoms in the DCMS process, which are beneficial for realizing a uniform film thickness [30]. To better understand the uniformity for the HiPIMS film, there are other significant aspects that should be considered, such as the target racetrack region of HiPIMS compared to that of DCMS, and the gas rarefaction effect in HiPIMS. Both these effects are related to the deposition rate of films and thus affect the uniformity of film deposition [20,31].

**3.2. XRD and EDS**

Fig.5 shows the typical XRD patterns of the titanium films deposited on the right side of the workpiece. The XRD patterns for the left side of the workpiece are similar to those for the right side and are therefore not included. XRD results reveal that all films contain polycrystalline titanium predominantly with a hexagonal structure; however, the films deposited under different conditions exhibit different preferential orientations of the lattice plane. The habit plane of titanium corresponds to (100), (002), and (101) for the $2\theta$ values in the range of 30°–45°. In this study, the ratio, $R_{hkl} = \frac{I_{hkl}}{I_{100} + I_{002} + I_{101}}$, was used to determine the preferential orientation of the lattice plane, wherein (hkl) takes the values (100), (002), and (101), and $I_{hkl}$ is the intensity of the (hkl) plane in XRD patterns. The $R_{hkl}$ values obtained from XRD results and those obtained from the International Center for Diffraction Data (ICDD; Reference code: 00-001-1197) are presented in Table 1. If the value of $R_{hkl}$ calculated using XRD patterns is higher than that obtained from the ICDD (Reference code: 00-001-1197), it implies that the (hkl) plane is the preferential lattice orientation. The higher the value of $R_{hkl}$, the higher the degree of preferential orientations [32]. Table 1 shows the

data of $R_{hkl}$ related to the preferential lattice orientation, marked with "*". Overall, the most prominent are the patterns from the (002) lattice plane. For the HiPIMS process, the titanium film exhibits a preferential lattice orientation of (002) at each deposition angle on the inner surface. On the outer surface, it also shows a (002) preferential orientation at lower deposition angles (such as M-0°) and (100) and (002) preferential orientations at high deposition angles (such as R-90°). During the HiPIMS process, positively ionized target atoms have a higher energy and atomic mobility under the external electric field, which is helpful for the preferential growth of the lattice plane with a low surface energy. The (002) crystal plane is a close-packed plane with the lowest surface energy [33]. However, for the DCMS process, except for the (002) preferential lattice orientation, the film also shows (100) and (101) preferential orientations at lower and higher deposition angles, respectively. Hence, HiPIMS films show better uniformity in terms of crystal texture than that of DCMS films.

The composition of the DCMS and HiPIMS films were measured using EDS. Fig.6 is the typical EDS spectra of the DCMS and HiPIMS films. The strongest peak in EDS is a Si signal since it is from a Si substrate, and the overall Si content was not counted in the present test. As shown in Fig.6, in addition to titanium, a few other elements, such as oxygen, nitrogen, and carbon, are present in the films deposited using both technologies. Typically, the presence of oxygen, nitrogen, and carbon is attributed to the residual gas in the vacuum chamber during the film deposition process or to contamination possibly caused when films are exposed to ambient air. Additionally, another factor that may contribute to the oxygen signal could be the oxidized surface of silicon, which is a phenomenon that has been observed in our previous studies [34-35]. The actual oxygen content in Ti films is therefore not considered to be as high as that determined using EDS profiles. As shown in Fig.6, it was also found that the amount of oxygen in the HiPIMS film is higher than that in the DCMS film. The reason for the difference was related to the film deposition rate. As discussed in Section 3.1, the HiPIMS film repeatedly has a lower deposition rate than that of the DCMS film, and this lower

deposition rate is more favorable for the residual oxygen within the vacuum chamber to accumulate on the film [37]. Furthermore, it was also found that when films were deposited using the same method, whether on the inner or outer surface, their EDS profiles were approximately the same; hence, they were not included in this report.

### 3.3. Cross-sectional morphology (SEM)

Fig.7 shows the typical cross-sectional morphology of titanium films deposited at lower and higher deposition angles on the left side of the workpiece. The resulting images for the right side of the workpiece are similar to those for the left side; hence, they are not shown here. It can be observed that the DCMS films at lower deposition angles exhibit a columnar structure perpendicular to the surface of the substrate, as shown in Figs.7a and 7b. However, at higher deposition angles, DCMS films grow on the substrate at an oblique angle, both on the inner and outer surfaces, as shown in Figs.7i and 7j. The obliquely grown film also shows some voids in the columnar grain structure, indicating that these areas of the film are relatively less dense than those deposited normal to the target. However, for the HiPIMS process, the titanium film always grows perpendicular to the substrate, both at lower and higher deposition angles, as shown in Figs.7c, 7d, 7k, and 7l. These films appear to be very dense both on the inner and outer surfaces. It is therefore reasonable to consider that the highly porous structure of DCMS films at higher deposition angles was mainly caused by the self-shadowing effect during oblique incidence deposition. However, the self-shadowing effect was almost suppressed during HiPIMS. During HiPIMS discharge, most sputtering atoms are charged particles, and their trajectory is modulated by the external electric field near the substrate. Simultaneously, the energy of the incident particles (including metal and argon ions) on the substrate is also enhanced by the electric field, which increases the adatom mobility and particle bombardment effect. Both effects contribute to the denser films deposited using HiPIMS compared to those deposited using DCMS.

### 3.4. Film hardness

The hardness of the titanium films deposited at different deposition angles on the inner and outer surfaces of the bowl-shaped workpiece are shown in Figs.8a and 8b, respectively. It is known that quite a few factors will affect the measured hardness of a deposited film, such as sputtering power, bias voltage, and even the (nano)indentation techniques used to measure hardness. There is limited published literature on the hardness of pure Ti films; however, in a few publications, the reported hardness of Ti-films varies from 2.4~10 GPa depending on the deposition method, coating thickness and crystallographic orientation [20,38-45]. It is also noticeable that DCMS sputtered films being found to have a lower hardness (~8GPa) than EB-evaporated films (~10GPa) in the study of Arshi et al [45] . In this study, as shown in Figs.8a and 8b, the titanium film deposited by DCMS agree with those values previously published for flat surfaces but decreases with increasing deposition angle. Interestingly the films deposited by HiPIMS reach hardness values comparable to those attainable by EB-evaporation and are much less sensitive to deposition angle. The range of hardness for Ti film reported in our study therefore falls within the hardness range reported in earlier literature for Ti-films. The reason for the range of hardness values recorded, in particular for DCMS-deposited films can be attributed to the effect of substrate shape (convex and concave) on the range of morphologies of the resulting films. Such effects have not been considered in other literature.

From Figs.8a and 8b, It can also be observed that the hardness of HiPIMS films at each deposition angle is consistently larger than that of DCMS films, both on the inner and outer surfaces. Furthermore, the hardness of DCMS films considerably decreases with increasing deposition angles. This variation was less significant in the HiPIMS deposited films.

The equation, $N = \frac{H_{\min}}{H_{\max}} \times 100\%$, was used to quantitatively evaluate the uniformity of film hardness, where $H_{\min}$ and $H_{\max}$ represent the minimum and maximum hardness on the same

surface, respectively. The hardness uniformity values of the DCMS films on the inner and outer surfaces were calculated to be 36.4% and 41.0%, respectively. Those of the HiPIMS films on the inner and outer surfaces were calculated to be 83.3% and 90.5%, respectively, as shown in Fig.9. The calculated results indicate that the hardness uniformity of HiPIMS films is very high and considerably better than that of DCMS films, on both the inner and outer surfaces. Additionally, for films prepared using the same method, the hardness uniformity of the film on the convex surface is slightly higher than that of the film on the concave surface. The mechanical properties of a material are also influenced by its microstructure and crystal texture. As mentioned in Sections 3.2 and 3.3, HiPIMS films show a uniform and compact microstructure. They exhibit a uniform preferential orientation of the (002) plane, which is a close-packed plane. However, DCMS films show a porous structure at higher deposition angles because of the self-shadowing effect in oblique incidence deposition. Their preferred orientation crystal plane also changes with deposition angles. The above factors provide a clear explanation as to why HiPIMS films have higher hardness and better uniformity than those of DCMS films when deposited on complex surfaces.

## 4. Conclusions

The uniformity of the titanium films deposited on the inner (concave) and outer (convex) surfaces of a bowl-shaped workpiece using both DCMS and HiPIMS methods was investigated. The deposition rate, crystal texture, microhardness, and microstructure were studied. Among these characteristics, the uniformity of the deposition rate on the bowl-shaped workpiece was most significantly affected by the surface shape of the substrate. This study showed that the uniformity of the film deposition rate on the concave surface was much higher than that of the film deposition rate on the convex surface in both DCMS and HiPIMS methods. The effect of the surface shape on film uniformity is a combination of the substrate-to-target distance, line of sight and the electric field near the substrate. Considering

the different deposition methods, HiPIMS films exhibited significantly better uniformity than that of DCMS films in terms of their deposition rate, film hardness, crystal texture, and microstructure, on both the concave and convex surfaces. The reason for the difference between the HiPIMS and DCMS films is that the HiPIMS method can significantly reduce the self-shadowing effect in oblique incidence deposition. This enhances the particle bombardment effect on the substrate, subsequently increases film densities, and eventually enhances deposited films through increasingly uniform structures and beneficial properties on complex-shaped workpieces.

This study contributes to the full analysis of the uniformity of the thickness, structure, and other properties of a film on a complex-shaped workpiece with both convex and concave surfaces. It is not only very helpful to correctly evaluate the service life of the film-modified workpiece, but it can inspire us to propose a solution for the weakest area of film. As discussed in Section 3.1, when a film is deposited on the concave surface, it is found that the deposition rate when using both the HiPIMS and DCMS methods exhibits different distribution trends. The deposition rate of DCMS films increases with increasing deposition angles but that of HiPIMS films exhibits an opposite trend. Therefore, we propose that films being alternately deposited using DCMS and HiPIMS should be a feasible solution to improve the uniformity of the film thickness on a concave surface.

It is known that gas pressure changes the ion energy distribution which hence could influence the uniformity of the deposited films[37]. The the effect of working gas pressure on the uniformity of film (including metal films and ceramic films) deposited on complex bowl-shaped workpiece is an on-going study, and the related results will be reported in a subsequent article.

**Acknowledgments**

This work was supported by the Science and Technology on Surface Physics and Chemistry Laboratory [grant number 6142A02190402]; the National Natural Science Foundation of

China [grant number 51975564]; and Chongqing Key Laboratory of Materials Surface & Interface Science [grant number KFJJ2008].

**References**

1.Kelly P J, Arnell R D. Magnetron sputtering: a review of recent developments and applications Vacuum, 2000, 56(3): 159-172.

2.Vick D, Friedrich L J, Dew S K, Brett M J, Robbie K, Seto M, and Smy T. Self-shadowing and surface diffusion effects in obliquely deposited thin films[J]. Thin Solid Films, 1999, 339(1–2):88-94.

3.Barranco A, Borras A, Gonzalez-Elipe A R, Palmero A. Perspectives on oblique angle deposition of thin films: From fundamentals to devices[J]. Progress in Materials Science, 2016, 76:59-153.

4.Jiang F, Zhang T F, Wu B H, Yu Y, Wu Y P, Zhu S F, Jing F J, Huang N, Leng Y X. Structure, mechanical and corrosion properties of TiN films deposited on stainless steel substrates with different inclination angles by DCMS and HPPMS[J]. Surface & Coatings Technology, 2016, 292:54-62.

5.Saksorn L, Pitak E, Chatchai P, Nat K, Metri H, Comparative investigations of DCMS/HiPIMS reactively sputtered WO3 thin films for photo-electrochemical efficiency enhancements, Vacuum, 2021, 185:109978

6.J.T. Gudmundsson.The high power impulse magnetron sputtering discharge as an ionized physical vapor deposition tool,Vacuum,2010, 84(12): 1360-1364.

7.Li C W, Tian X B, Gong C Z, Xu J P, Liu S X. Synergistic enhancement effect between external electric and magnetic fields during high power impulse magnetron sputtering discharge, Vacuum,2017, 143:119-128,.

8.Ganesan R, Akhavan B, Dong X, McKenzie D R, Bilek M M M. External magnetic field increases both plasma generation and deposition rate in HiPIMS[J]. Surface & Coatings Technology, 2018, 340.

9.Li C, Tian X b, Liu T, Li T W, Qin J W, Yang J J, Guo C Z, Yang S Q. Study on Vanadium Films Deposited on Concave Object by Conventional Direct Current and High Power Pulsed Magnetron Sputtering[J]. Rare Metal Materials & Engineering, 2013, 42(12):2437-2441.

10.Shimizu T, Komiya H, Teranishi Y, Morikawa K, Nagasaka H, Yang M. Pressure dependence of (Ti, Al)N film growth on inner walls of small holes in high-power impulse magnetron sputtering[J]. Thin Solid Films, 2017: 189-196.

11.Bobzin K, Bagcivan N, Immich P, Bolz S, Alami J and Cremer R. Advantages of nanocomposite coatings deposited by high power pulse magnetron sputtering technology[J]. Journal of Materials Processing Technology, 2009, 209(1): 165-170.

12.Bagcivan N, Bobzin K, Theis S. Comparison of (Cr0.75Al0.25)N Coatings Deposited by Conventional and High Power Pulsed Magnetron Sputtering[J]. Contributions To Plasma Physics, 2012, 52(7): 601-606.

13. Sarakinos K , Alami J , Konstantinidis S . High power pulsed magnetron sputtering: A review on scientific and engineering state of the art[J]. Surface & Coatings Technology, 2010, 204(11):1661-1684.

14.Decorative Paints Market Forecast to 2028 - COVID-19 Impact and Global Analysis by Type and Application,2021.
https://apnews.com/press-release/business-wire/4354cd74c9404d69899bf6514991c414

15.Elias C N, Lima J H, Valiev R Z, Meyers M A. Biomedical applications of titanium and its alloys[J]. JOM, 2008, 60(3): 46-49.

16.Balyanov A, Kutnyakova J, Amirkhanova N A, Stolyarov V V, Valiev R Z, Liao X Z, Zhao Y H, Jiang Y B, Xu H F, Lowe T C. Corrosion resistance of ultra fine-grained Ti[J]. Scripta Materialia, 2004, 51(3):225-229.

17.Wu B H, Chen S, Wu J, Leng Y X, Xie D, Jiang F, Huang N, Sun H. Titanium interlayer between Ti–O film on CoCrMo implant alloy for improving adhesion: Detailed XPS and TEM analysis of the interface[J]. Surface & Coatings Technology, 2015, 277(6):197-202.

18.Chen S, Wu B H, Xie D, Jiang F, Liu J, Sun H L, Zhu S F, Bai B, Leng Y X, Huang N. The adhesion and corrosion resistance of Ti–O films on CoCrMo alloy fabricated by high power pulsed magnetron sputtering (HPPMS)[J]. Surface & Coatings Technology, 2014, 252(9):8-14.

19. Ali Shanaghi, Paul K. Chu, Ruizhen Xu, Tao Hu, Structure and properties of TiC/Ti coatings fabricated on NiTi by plasma immersion ion implantation and deposition, Vacuum,2013, 89: 238-243.

20.F.J. Jing, T.L. Yin, K. Yukimura, H. Sun, Y.X. Leng, N. Huang,Titanium film deposition by high-power impulse magnetron sputtering: Influence of pulse duration, Vacuum,2012,86(12): 2114-2119.

21. J Alami，V Stranak，AP Herrendorf，Z Hubicka，R Hippler, Design of magnetic field configuration for controlled discharge properties in highly ionized plasma[J]. Plasma Sources Science Technology, 2015, 24(4):045016.

22.V. Stranak, R. Bogdanowicz, S. Drache, M. Cada, Z. Hubicka and R. Hippler, Dynamic Study of Dual High-Power Impulse Magnetron Sputtering Discharge by Optical Emission Imaging, IEEE Transactions on Plasma Science, 2011, 39(11):2454-2455

23.Anders A. Deposition rates of high power impulse magnetron sputtering: Physics and economics[J]. Journal of Vacuum Science & Technology A Vacuum Surfaces & Films, 2010, 28(4):783.

24.Brenning N, Butler A, Hajihoseini H, Rudolph M, Raadu M A , Gudmundsson J T, Minea T, Lundin D. Optimization of HiPIMS discharges: The selection of pulse power, pulse length, gas pressure, and magnetic field strength[J]. Journal of Vacuum Science & Technology A Vacuum Surfaces and Films, 2020, 38(3):033008.

25.Jeong S H, Boo J H. Influence of target-to-substrate distance on the properties of AZO films grown by RF magnetron sputtering[J]. Thin Solid Films, 2004, s 447–448(448):105-110.

26.Chun-Wei Li, Tian X B, Gong C Z, Xu J P. Microstructure and Thickness Uniformity of Vanadium Films on Concave Object at Different Target-Substrate Distance by HiPIMS[J]. Surface Technology, 2016.

[27]Nakano T , Yamazaki R , Baba S . Effects of Atomic Weight, Gas Pressure, and Target-to-substrate Distance on Deposition Rates in the Sputter Deposition Process[J]. Journal of the Vacuum Society of Japan, 2014, 57(4):152-154.

28.Hippler R, Hubicka Z, Cada M, Ksirova P, Wulff H, Helm C A, Stranak V. Angular dependence of plasma parameters and film properties during high power impulse magnetron sputtering for deposition of Ti and TiO 2 layers[J]. Journal of Applied Physics, 2017, 121(17):171906.

29.Jing H , Gong C Z, Tian X B, Yang S Q. Uniformity of TiN Films Fabricated by Hollow Cathode Discharge[J]. Plasma Science and Technology, 2010, 12(2):212-217.

30. Liu Y , Chen Y . Synthesis of large scale graphene oxide using plasma enhanced chemical vapor deposition method and its application in humidity sensing[J]. Journal of Applied Physics, 2016, 119(10):666-669.

31.Raman P，Shchelkanov I，Mclain J，Cheng M，Ruzic D，Haehnlein I，Jurczyk B，Stubbers R，Armstrong S.High Deposition Rate Symmetric Magnet Pack for High Power Pulsed Magnetron Sputtering,Surface and Coatings Technology,2016, 293:10-15

32.Matsushima H, Nohira T, Mogi I, Ito Y. Effects of magnetic fields on iron electrodeposition[J]. Surface & Coatings Technology, 2004: 245-251.

33.Song Y H, Cho S J, Jung C K, Bae I S, Boo J H, Kim S. The Structural and Mechanical Properties of Ti Films Fabricated by Using RF Magnetron Sputtering[J]. Journal- Korean Physical Society, 2007, 51(3):1152-1155.

34. Lin S X, Xie D, Tang Y L, Wang Y W, Jing F J, Huang N, Leng X Y. Effect of nitrogen flow on the properties of carbon nitride films deposited by electron cyclotron resonance plasma-enhanced chemical vapor deposition, Vacuum,2021, 189:110223

35. Ganesan R, Murdoch B J, Partridge G J, Bathgate S, Treverrow B, Dong X, Ross A E, McCulloch D G, McKenzie D R, Bilek M M M, Optimizing HiPIMS pressure for deposition of high-k (k=18.3) amorphous $HfO_2$, Applied Surface Science, 2016, 365: 336-341

36. Geng X, Liang H, Li W J, Parsapinto A, Thiry D, Chen M F, Snyders R. Experimental evaluation of the role of oxygen on the growth of MgOx nano-sculpted thin films synthesized by reactive magnetron sputtering combined with glancing angle deposition, Thin Solid Films, 2021,718: 138480

37.Hippler R, Cada M, Stranak V, Helm C A, and Hubicka Z. Pressure dependence of singly and doubly charged ion formation in a HiPIMS discharge", Journal of Applied Physics ,2019,125, 013301

[38] Moskovkin P, Maszl C, Schierholz R, Breilmann W, Petersen J, Pflug A, Muller J, Raza M, Konstantinidis S, Keudell A V, Lucas S. Link between plasma properties with morphological, structural and mechanical properties of thin Ti films deposited by high power impulse magnetron sputtering,Surface and Coatings Technology,2021,418,127235.

[39]Zhang H K, Li X, Su J Y, Wang X L, Ma L Z, Xue J W, Li Y H, Song Z X. Modulation of columnar crystals of magnetron sputtered Ti thin films,Thin Solid Films,2019,689,137512,

[40]Liu Y L, Liu F, Wu Q, Chen A Y, Li X, Pan D. Effect of bias voltage on microstructure and nanomechanical properties of Ti films,Transactions of Nonferrous Metals Society of China,2014,249(9):2870-2876

[41] Fazio M, Vega D, Kleiman A, Colombo D, Franco Arias L M, Márquez A. Study of the structure of titanium thin films deposited with a vacuum arc as a function of the thickness, Thin Solid Films,2015, 593:110-115

[42]Jeyachandran Y L, Karunagaran B, Narayandass Sa K, Mangalaraj D, Jenkins T E, Martin P J. Properties of titanium thin films deposited by dc magnetron sputtering, Materials Science and Engineering: A, 2006,431(1-2):277-284

[43]Baohua W, Yan Y, Jian W, Ivan S, David N R, Nan H, Yongxiang L.Tailoring of titanium thin film properties in high power pulsed magnetron sputtering. Vacuum, 2018, 150:144-154

[44]Chang R C , Chen F Y , Chuang C T, Tung Y C. Residual stresses of sputtering titanium thin films at various substrate temperatures. Journal of Nanoscience & Nanotechnology, 2010, 10(7):4562-4567

[45]Arshi N, Lu J Q, Lee C G, Yoon J H, Koo B H, Ahmed F. Thickness effect on properties of titanium film deposited by d.c. magnetron sputtering and electron beam evaporation techniques. Bulletin of Materials Science, 2013, 36(5):807-812

Table i. Ratio of $R_{hkl} = \frac{I_{hkl}}{I_{100} + I_{002} + I_{101}}$ for the XRD patterns shown in Fig.5

| Position | Lattice plane | | |
|---|---|---|---|
| | (100) | (002) | (101) |
| DCMS(inner)-M-0° | 0.40* | 0.51* | 0.09 |
| DCMS(inner)-R-60° | 0 | 0.61* | 0.39 |
| DCMS(inner)-R-90° | 0 | 0.25* | 0.75* |
| DCMS(outer)-M-0° | 0.39* | 0.51* | 0.1 |
| DCMS(outer)-R-60° | 0.48* | 0.43* | 0.09 |
| DCMS(outer)-R-90° | 0 | 0.24* | 0.76* |
| HiPIMS(inner)-M-0° | 0.04 | 0.94* | 0.02 |
| HiPIMSS(inner)-R-60° | 0.05 | 0.92* | 0.03 |

| | | | |
|---|---|---|---|
| HiPIMS(inner)-R-90° | 0.05 | 0.93* | 0.02 |
| HiPIMS(outer)-M-0° | 0.07 | 0.87* | 0.06 |
| HiPIMS(outer)-R-60° | 0.51* | 0.49* | 0 |
| HiPIMS(outer)-R-90° | 0.53* | 0.47* | 0 |
| ICDD(Ref.Code. 00-001-1197) | 0.22 | 0.22 | 0.56 |

**Figure Captions**

Fig. 1. Schematic of the vacuum deposition system

Fig. 2. Experimental arrangement and location of Si wafers (L for left, M for middle, and R for right; figures indicate the deposition angle with respect to the surface normal of the cathode). (a) Inner and (b) outer surfaces of the bowl-shaped workpiece

Fig. 3. Distribution of the film deposition rate on (a) inner and (b) outer surfaces of the bowl-shaped workpiece using DCMS and HiPIMS, respectively

Fig. 4. Uniformity of the Ti film deposition rate on the inner and outer surfaces of the bowl-shaped workpiece using DCMS and HiPIMS

Fig. 5. XRD patterns of titanium films deposited at different deposition angles on the inner and outer surfaces of the workpiece using (a) DCMS and (b) HiPIMS

Fig. 6. EDS profiles of the titanium film for (a) DCMS (outer)-M-0° and (b) HiPIMS (outer)-M-0°

Fig. 7. Cross-sectional morphology of titanium films deposited using DCMS at (a) inner surface M-0°, (e) inner surface L-60°, (i) inner surface L-90°, (b) outer surface M-0°, (f) outer surface L-60°, (j) outer surface L-90°, and deposited via HiPIMS at (c) inner surface M-0°, (g) inner surface L-60°, (k) inner surface L-90°, (d) outer surface M-0°, (h) outer surface L-60°, and (*l*) outer surface L-90°, respectively

Fig. 8. Distribution of the film hardness on (a) inner and (b) outer surfaces of the bowl-shaped workpiece using DCMS and HiPIMS, respectively

Fig. 9. Uniformity of the film hardness on the inner and outer surfaces of the bowl-shaped workpiece

**Figures**

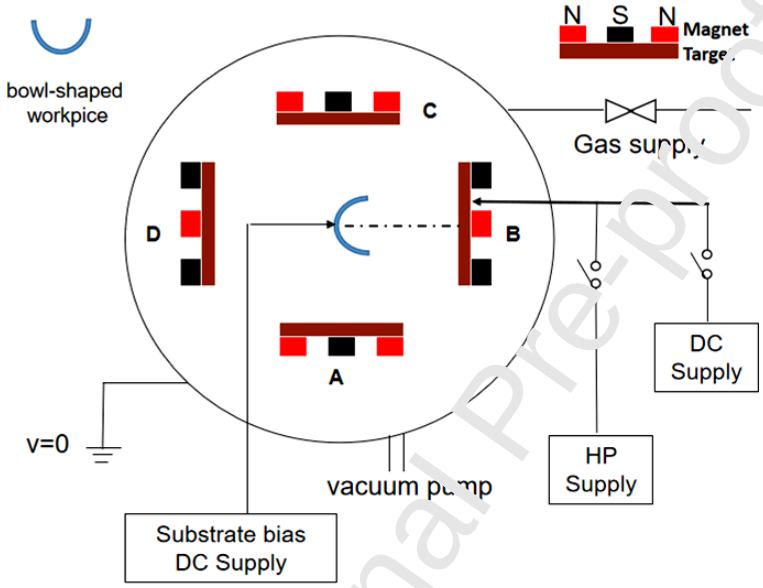


Fig.1

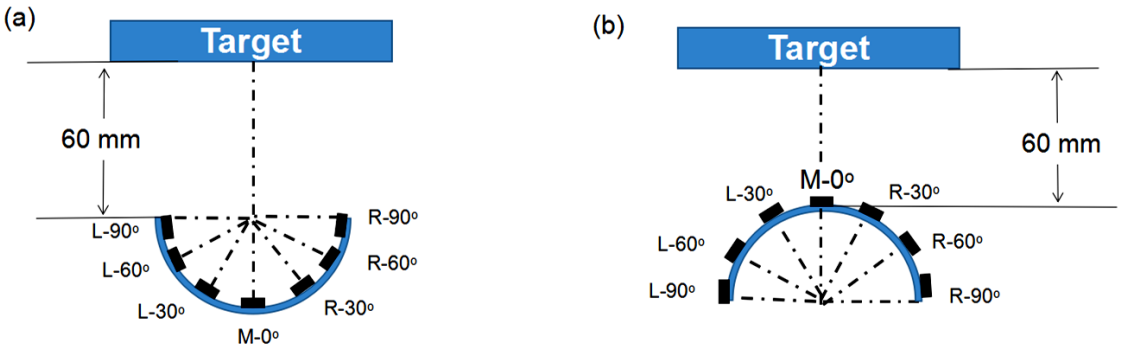


Fig.2

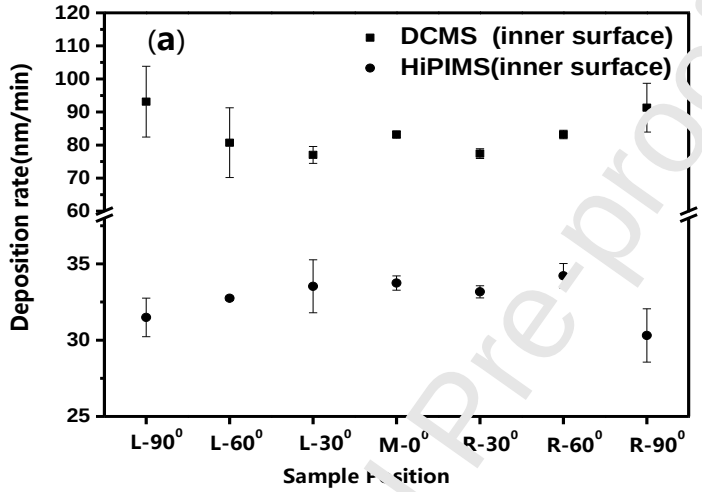


Fig.3a

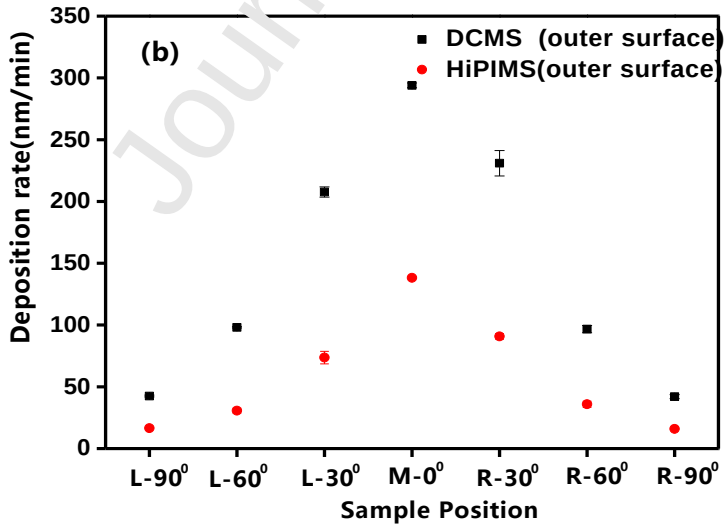


Fig.3b

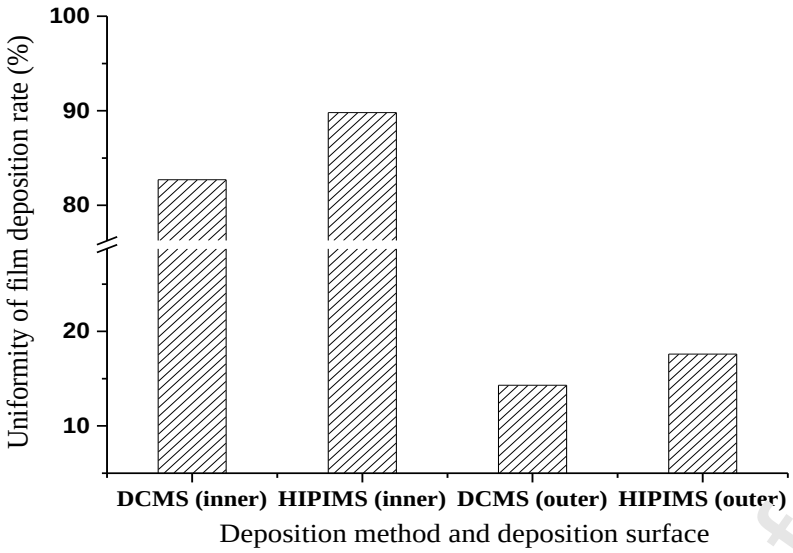


Fig.4

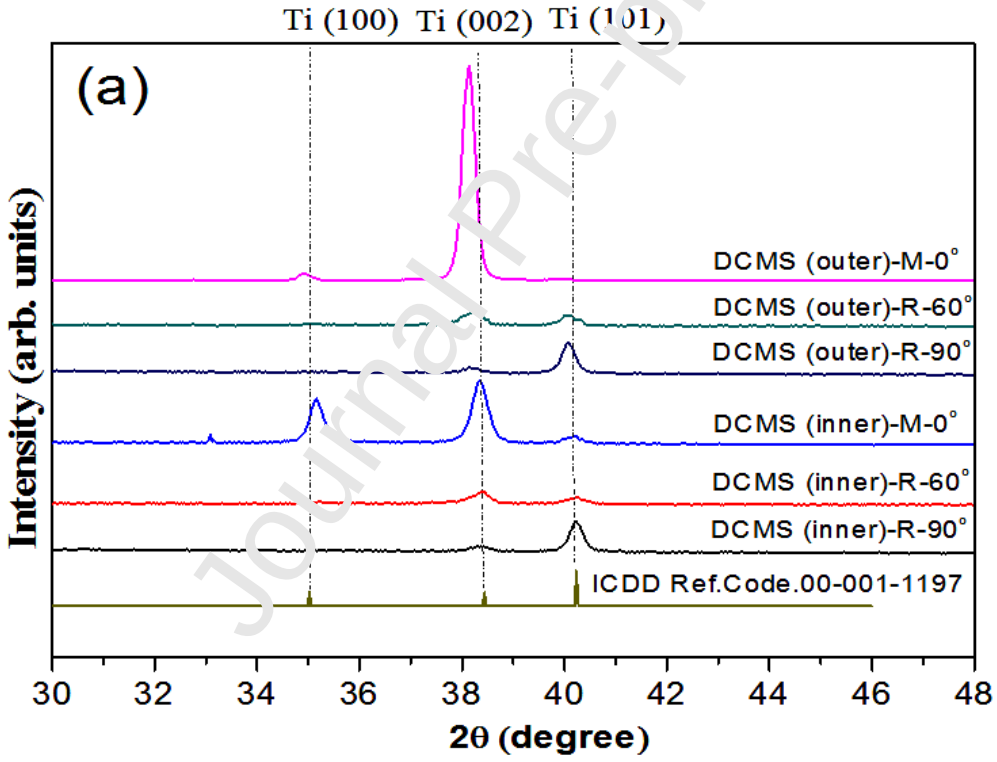


Fig.5a

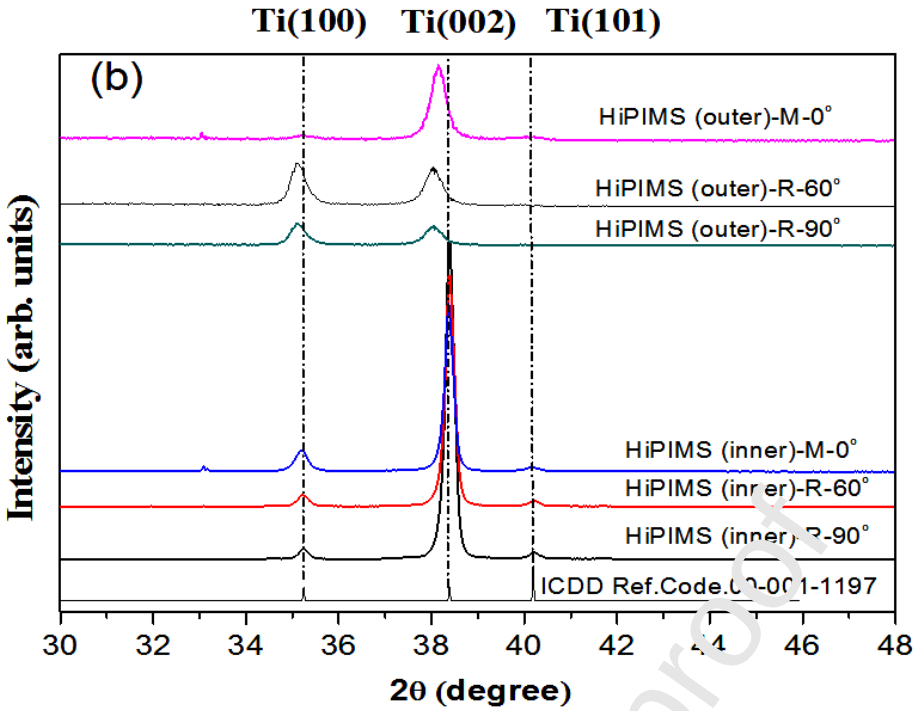


Fig.5b

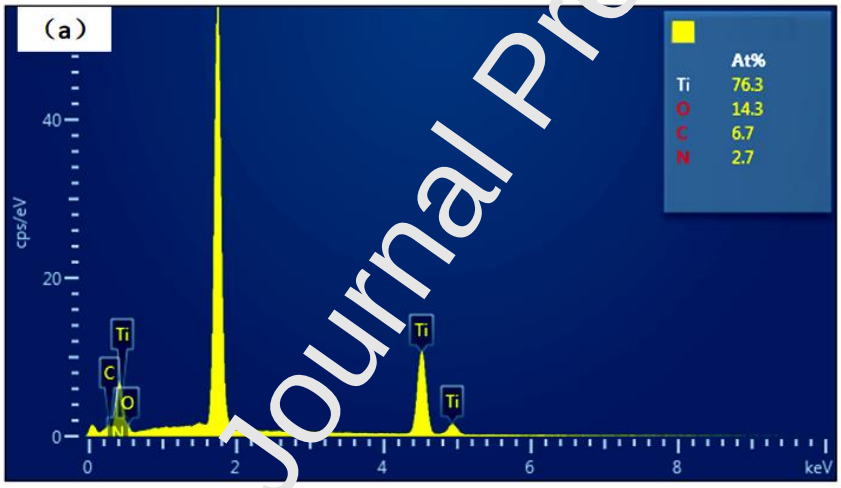


Fig.6a

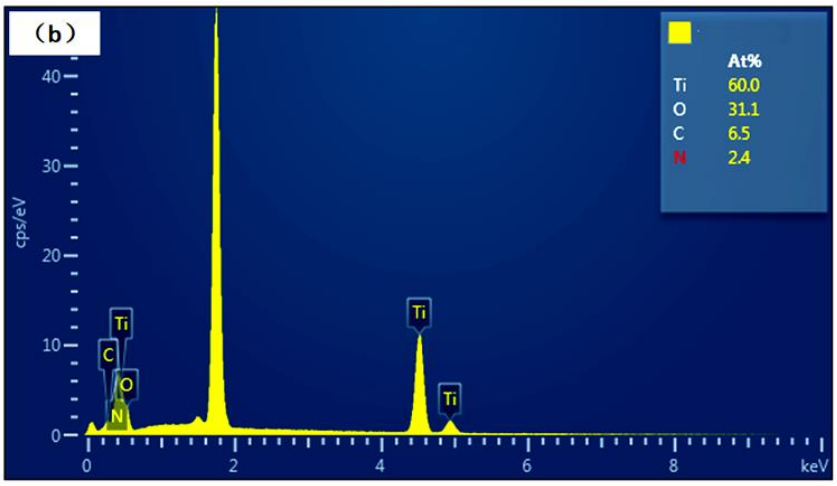


Fig.6b

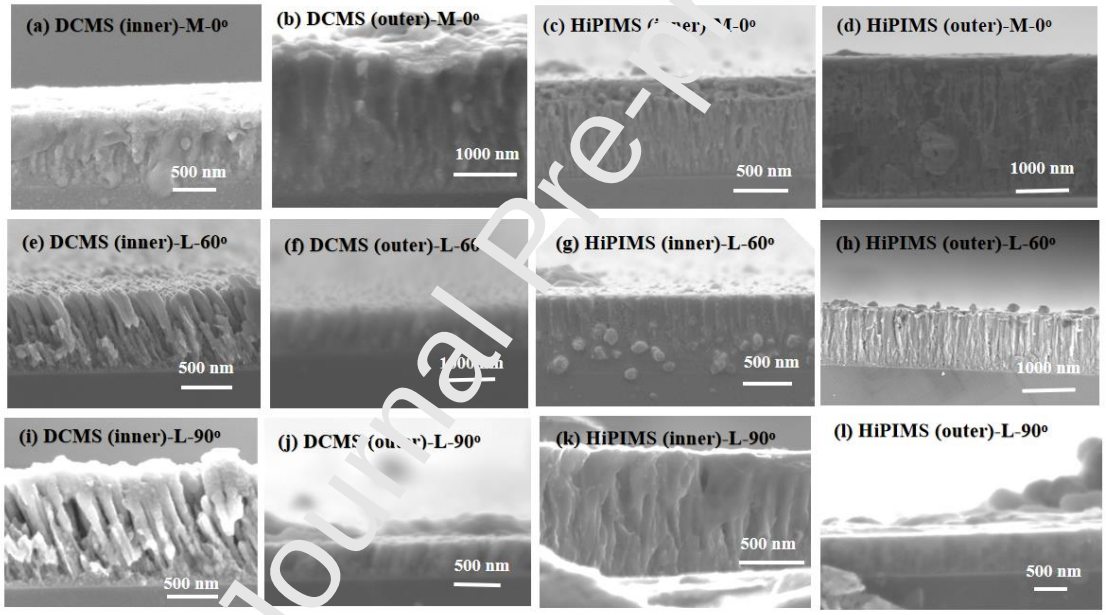


Fig.7

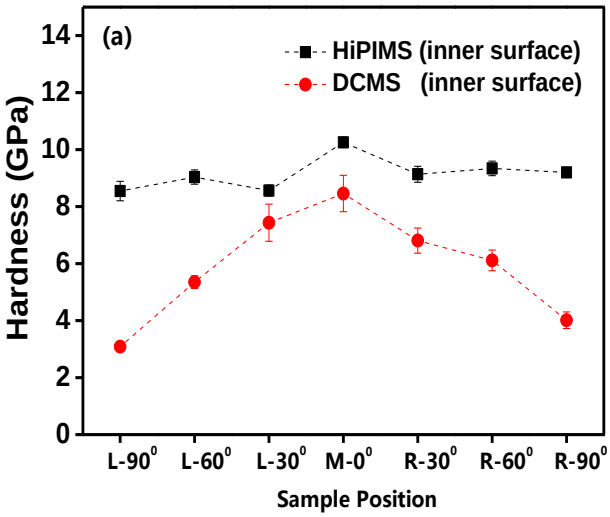


Fig.8a

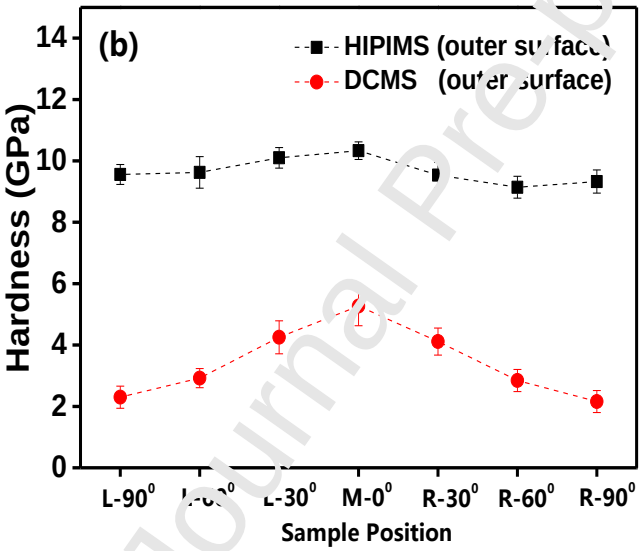


Fig.8b

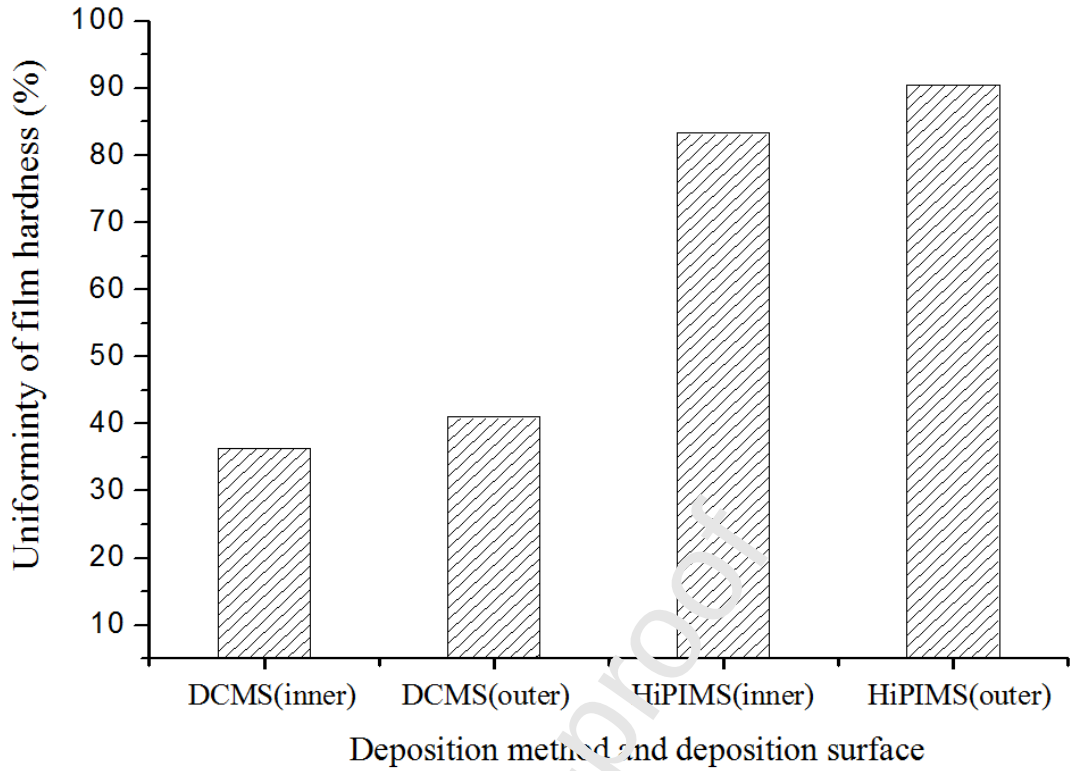


Fig.9

**Declaration of interests**

☒ The authors declare that they have no known competing financial interests or personal relationships that could have appeared to influence the work reported in this paper.

☐The authors declare the following financial interests/personal relationships which may be considered as potential competing interests:

**Credit author statement**

**Dong Xie:** Conceptualization, Writing - Review & Editing, Funding acquisition

**L.J. Wei:** Investigation,Writing - Original Draft,

**H.Y.Liu:** Resources，Validation

**K. Zhang:** Methodology

**Y.X. Leng:** Supervision，Project administration

**YD.T.A. Matthews:** Writing - Review & Editing

**R. Ganesan:** Writing - Review & Editing

**Y.Y. Su**：Data Curation

## Highlights

- Titanium films were deposited via DCMS and HiPIMS on bowl-shaped workpiece.
- Surface shape (Convex or concave ) influence the uniformity of film deposition rate.
- HiPIMS films showed better uniformity in properties compared to DCMS films.
- HiPIMS reduced the self-shadowing effect in oblique incidence deposition.